Chemical Vapor Deposition in a Partitioned Box Reactor

J. J. Bernstein*

The Charles Stark Draper Laboratory, Cambridge, Massachusetts 02139

ABSTRACT

The partitioned box reactor, a novel high throughput CVD reactor, is presented. The reactor has good chemical and energy efficiency, and the large surface/volume ratio results in suppression of homogeneous nucleation. The scaling behavior of gas flow and the various deposition regions (surface rate limited, diffusion limited, and depletion limited) are discussed. Experimentally obtained maps of static and integrated deposition profiles are given for carbon and silicon films.

The partitioned box reactor consists of a rectangular cross-sectional tube divided into narrow rectangular channels by a series of partitions (Fig. 1). A similar reactor has been used to deposit epitaxial GaAs in a multiwafer CVD reactor (1). Several of these boxes can be placed end-to-end in a multibox system, which is enclosed in a quartz tube to contain the reactant gases (Fig. 2). A short furnace is scanned over the boxes to achieve uniform deposition over the internal surfaces of the reactor.

The closely spaced partitions give the reactor a large surface to volume ratio, resulting in the following unique and desirable properties: (*i*) a large surface area is coated in a small volume reactor, (*ii*) gases exit near thermodynamic equilibrium, implying efficient chemical utilization, (*iii*) homogeneous nucleation (particulate formation) is suppressed, (*iv*) insulation of the reactor results in high energy efficiency, (*v*) pressure drop through the channels results in self-manifolding of the gas flow, (*vi*) coatings of high uniformity are possible by motion of the hot zone relative to the boxes. It is interesting to compare this reactor to a typical cold wall CVD reactor used to deposit (for example) polycrystalline silicon on silicon wafers. The partitioned box reactor utilizes far less reactant chemicals and far less energy to deposit a given amount of silicon, because it efficiently brings together reactant gases, energy and surfaces for deposition in a small volume.

In the body of this paper the scaling properties of this reactor will be derived by dimensional analysis. Experimental results will be presented on the deposition at atmospheric pressure of high purity films of carbon and silicon. These films were used as feedstock in a solar cell process (2, 3). Highly uniform films of Si_3N_4, SiO_2, and SiC were also grown successfully in this reactor.

Gas Flow in a Partitioned Box

The gas flow in the channel formed between two partitions is shown in Fig. 3. The narrow spacing h (called the gap) causes a low Reynolds number and hence laminar flow. Using the simplifying assumption of constant temperature and neglecting edge effects where the partitions are held by the box, the Navier-Stokes equation (4) can be simplified to yield one-dimensional parabolic flow

$$v_x = -\frac{1}{\mu}\frac{dP}{dx}\left(\frac{h^2}{8} - \frac{z^2}{2}\right) \qquad [1]$$

where the coordinate system is shown in Fig. 3. μ is the viscosity, and the origin is taken in the center of the gap. The peak velocity is

$$v_O = -\frac{dp}{dx}\frac{h^2}{8\mu} \qquad [2]$$

while the average (or cup-mixing) velocity is $\langle v \rangle = 2/3\, v_O$. The total gas flow through one channel is

$$V = ab\langle v \rangle = -\frac{\Delta p}{12\mu}\left(\frac{h^3 b}{c}\right) \qquad [3]$$

where Δp is the pressure drop along a channel of length c and width b. The pneumatic resistance of one channel is

$$R = \frac{\Delta p}{V} = \frac{12\mu c}{h^3 b} \qquad [4]$$

Note that the resistance to flow varies as the inverse cube of the gap, whereas in a cylindrical pipe the flow is inversely proportional to the fourth power of the diameter. Plexiglas partitioned boxes and smoke generators were used to aid flow visualization during the design process.

Edge effects where the partitions are held in place by the box grooves perturb the flow for a distance of approximately $2h$ from the edges at $y = 0$ and $y = b$ (Fig. 4). A region of uniform deposition (within 95% of center thickness) is observed experimentally over a width of b-$4h$. Reduced deposition in the edge region of width $2h$ is caused by the presence of the box side which reduces the gas velocity (reducing the supply of reactants) and competes for the depositing substance.

The closely spaced channels in a partitioned box offer considerable resistance to flow. This causes the boxes themselves to be self-manifolding, so that the reactant gases divide themselves evenly between all available channels. This in turn places demands on the dimensional tolerances of the partition thickness, flatness, and grooved box machining. As Eq. [3] shows, a 1% variation in h could cause a 3% variation in gas flow and therefore deposit thickness. In a later section of this paper thickness maps of actual depositions on nonparallel partitions will be shown which demonstrate the influence of h on deposit thickness.

The pneumatic resistance of a box increases rapidly with temperature. Assuming that the gas expands in proportion to temperature, and that the viscosity is proportional to

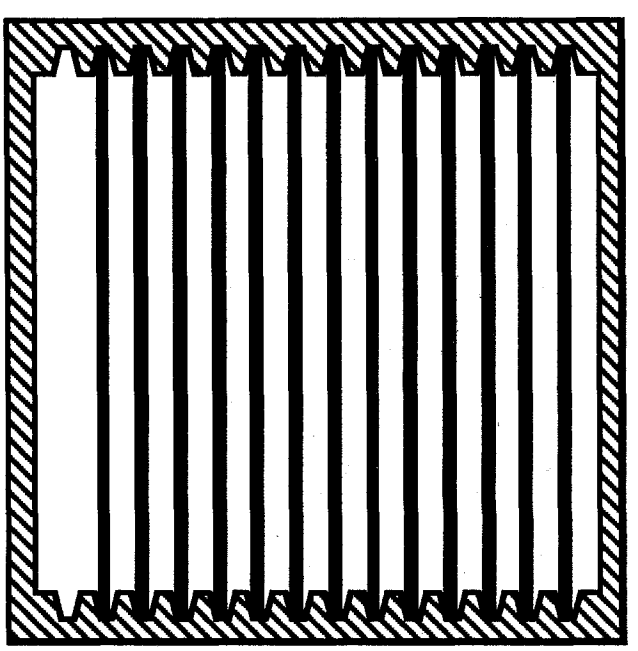

Fig. 1. Cross-sectional view of a partitioned-box reactor, showing grooved box, partitions, and one empty slot. Gas flow is out of the page.

*Electrochemical Society Active Member.

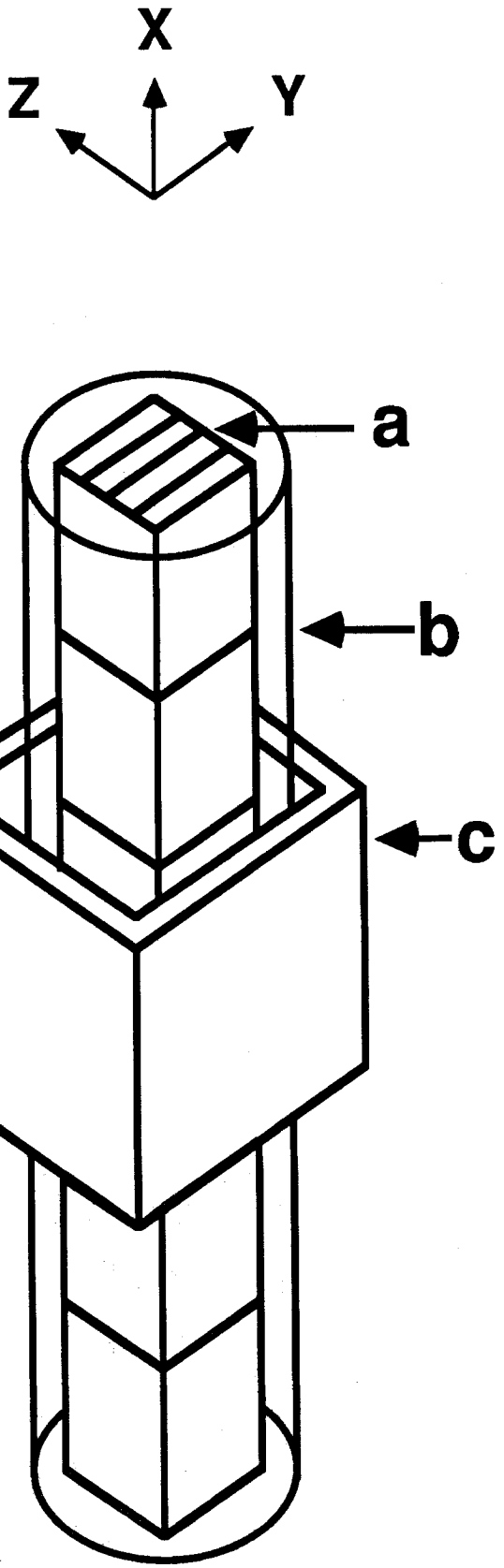

Fig. 2. Partitioned-box reactor, showing (a) stack of partitioned boxes, (b) quartz containment tube, and (c) short moving furnace.

$T^{1/2}$, (*i.e.*, ideal gas), then the pneumatic resistance increases as $T^{3/2}$. For a gas heated from $T = 0°$-1000°C, this causes a ten-fold increase in resistance and pressure drop. This is a greatly simplified view of the problem because the temperature, the chemical composition, and the viscosity of the reacting gases have a complex three-dimensional distribution. No attempt at a complete analytical or finite element model was made, however, important conclusions about scaling behavior can be reached with a relatively simple model.

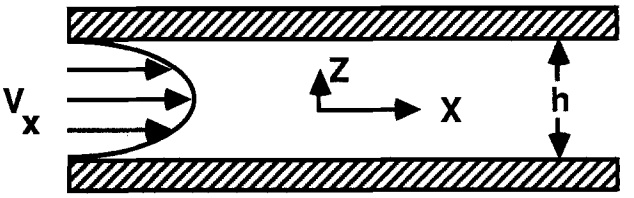

Fig. 3. Laminar, parabolic flow in the channel formed between partitions.

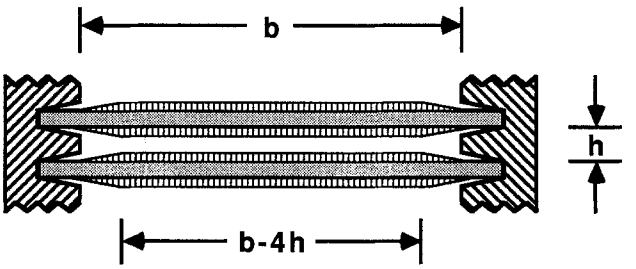

Fig. 4. Central region of uniform deposition has width *b-4h* due to edge effects (drawing not to scale).

Experimental

Partitioned boxes were machined from graphite, purified by 1200°C treatment in HCl, and then coated with pyrolytic carbon to reduce contamination, surface area, and adsorption. Various partition materials were used. Silicon partitions were sliced from Wacker Silso cast ingots. SiC materials from approximately ten vendors were investigated, including hot-pressed, reaction bonded, silicon filled, and sintered. The sintered-alpha material (Hexoloy) from Carborundum-Sohio proved by far the most durable and one of the most pure, although a boron compound is added to aid sintering. Boron autodoping from the partitions was much smaller than the intentional boron doping to 1 Ω-cm. These partitions were cleaned using solvent degreasing, H_2SO_4-H_2O_2 baths, 1200°C HCl-H_2O oxidations. This process created an oxide coating and an impurity-depleted surface skin by out-diffusion. The diffusion coefficient of most impurities through SiC at temperatures below 1100°C is so small that silicon sheets deposited on the SiC partitions were indistinguishable from sheets grown on semiconductor grade Si partitions. Analysis by SIMS, NAA, XRF, and spark source mass spectrometry showed that the purity of polysilicon grown on these substrates was comparable to that of float-zone Si wafers. The efficiencies of solar cells fabricated from these silicon sheets also failed to distinguish between the two partition materials, with the best cells showing a 13% efficiency.

Carbon films were typically deposited from 2% methane or 5% iso-propyl alcohol (IPA) in nitrogen at 1100°C, grown to a thickness between 1 and 2 μm. The short furnace (30 cm long) was scanned over a stack of eight boxes (total length 142 cm) at a rate of 1 cm/min until all the boxes were internally coated.

Silicon was deposited in the same reactor without unloading the substrates, by switching inlet gases to $SiHCl_3$ 8% in H_2. The $SiHCl_3$ was precisely metered using a micromotion liquid flow meter, and then fed into a heated vaporizer chamber where it was evaporated into the H_2 stream. All gas streams were metered by mass flow controllers. The entire deposition run, including mass flow controllers, furnace scan speed, and temperature was measured and controlled by an IBM PC using Keithley interface electronics.

Temperature was measured via a 2 μm infrared optical pyrometer (Vanzetti Corporation) using a fiber optic link to the moving furnace. The 2 μm detection wavelength was selected to be near the peak emission of the graphite boxes at 1100°C. The peak emission of the furnace quartz-halogen heater elements was at 1 μm. The choice of de-

tector wavelength, the high emissivity of the graphite boxes, and the use of a sight tube combined to give good rejection of spurious furnace radiation. Furnace induced temperature error, measured by suddenly shutting off the furnace, was less than 20°C, and was compensated by calibrating the pyrometer during test runs with thermocouples embedded in the boxes. Thus box temperature could be controlled to within 10°C.

After silicon deposition, the boxes were unloaded and the partitions were loaded in stacks into semiconductor oxidation furnaces at 1000°C. There, the carbon layers were oxidized, freeing the silicon sheets (2). The polysilicon sheets were zone melted with CO_2 lasers to increase grain size, and then used as feedstock in a solar cell process. The partitions and boxes were repeatedly cycled through the process.

Measurements of carbon film thickness were made with a surface profiler (Tencor alpha-step) on carbon coated partitions. Carbon film thickness was also inferred from four-point probe sheet resistance data using the measured resistivity of the pyrocarbon (1.3×10^{-3} Ω-cm). Silicon sheet thickness was measured after the oxidation undercut process using a dial gauge. Thickness maps of silicon and carbon depositions will be shown in the static and integrated deposition sections. Homogeneous nucleation during carbon deposition was found to be a problem, hence a separate section on its suppression has been included.

Suppression of Homogeneous Nucleation

During the CVD of pyrocarbon films, homogeneous nucleation (soot) can be a serious problem. Particles on the substrates during silicon deposition are engulfed in silicon and may not be oxidized during the burnout step, leading to undesirable carbon contamination in the product solar cells. The formation of pyrocarbon is an extremely complicated process, typically involving the formation of many thousands of organic compounds of increasing molecular weight and decreasing hydrogen/carbon ratio (6, 7). There still exists disagreement on the precise mechanisms of carbon formation, however, by varying the experimental conditions one can produce smooth films of pyrocarbon, soot, or tars and oils. Heterogeneous nucleation is favored over homogeneous nucleation because of the reduced energy barrier to nucleation. Sooting can be suppressed if the reacting gas is not required to diffuse too far to find a deposition surface. The following techniques were found useful in eliminating this problem.

1. Increasing the surface/volume ratio, by decreasing the partition spacing.

2. Decreasing the concentration of the hydrocarbon precursor. In practice, to gain a high deposition rate, the concentration is run just below the threshold for soot formation.

3. Choice of hydrocarbon precursor: many gases were studied, including CH_4, C_3H_8, $C_2H_3Cl_3$, and C_3H_7OH. Of these, isopropyl alcohol (IPA) was found to give the fastest soot-free deposition.

4. Furnace length and hot zone must be greater than several characteristic deposition lengths (derived in the next section), so that the exhaust gas contains no condensible hydrocarbons. If oil or tar vapors exit the furnace, they will condense as soot or oil films on the downstream partitions.

5. Increase the diffusion coefficient: a, LPCVD: some experiments were successfully carried out in vacuum, however, it was desired to deposit the carbon and the silicon in the same reactor, and the additional cost and complexity of a vacuum process made this seem unattractive. b, Use of He rather than N_2 as the carrier gas: The cost of He was considered prohibitive. It is interesting that H_2 used as a carrier gas suppresses pyrocarbon formation.

6. Heat the gases more slowly, allowing more time for diffusion to the walls. This can be achieved with a smaller thermal gradient at the furnace entrance, and by reducing the inlet gas velocity.

7. Avoid all contamination, especially from transition metals. It is well-known that traces of certain metals catalyze graphitic nodules and fibrous growth (7). It was essential to purify the graphite boxes with high temperature HCl treatments, and to avoid stainless steel tweezer marks on the deposition substrates.

Static Deposition Profiles

This section discusses deposition in a partitioned box in which the furnace is stationary with respect to the boxes. Surface reaction rate limited, mass transport limited, and depletion limited deposition zones are described. A characteristic deposition length L is derived, and data on static deposition of carbon and silicon are presented.

As the reactant gases pass upward through the partitioned boxes, almost nothing deposits until a minimum activation temperature is reached (Fig. 5). The deposition reaction then increases rapidly with temperature, typical of a thermally activated Arrhenius dependence. This low temperature entrance region is the surface reaction rate-limited region. As the temperature rises the surface reaction rate becomes faster than the diffusion of reactant to the surface, and the mass transport limited region is entered. The length of the surface reaction limited region is determined by the temperature gradient in the x direction. After a characteristic deposition length L (derived below), the gas becomes depleted. The exhaustion of all available reactant gas leads to an exponential decay of deposition of deposition rate, in contrast to the inverse square-root dependence typical of a boundary layer mass-transport limitation. This is called the depletion region, and is not found in most semiconductor CVD reactors. In most CVD reactors the characteristic deposition length L is larger than the reactor, gas depletion is not achieved, and most of the reactant gases are wasted. This large excess of reactant gases is necessary to achieve uniformity. In contrast, the gases exiting the partitioned-box reactant are close to thermodynamic equilibrium at the exit temperature, resulting in maximum gas utilization. Uniformity is achieved by moving the furnace relative to the boxes to integrate the static deposition.

The characteristic deposition length L is derived with reference to Fig. 3. An exact solution of the problem of deposition in a tube, annulus, or channel is known as the Graetz problem (5). The gas moves with average velocity $<v>$ through a channel of width h. The gas is assumed to react infinitely fast at the channel walls. Mass transport in the z direction is by diffusion only. The time required for a gas molecule to diffuse a distance $h/2$ is $h^2/4D$, where D is an average diffusion coefficient for the gas mixture. In this time the gas travels the characteristic deposition length

$$L = \frac{h^2 <v>}{4D} \qquad [5]$$

In the exact solution of the mass transport problem, distances are nondimensionalized by this characteristic length. Equation [5] shows again the critical importance of the plate spacing in determining the deposition zone length. For example, suppose that to increase reactor throughput it is proposed to halve the plate spacing. In

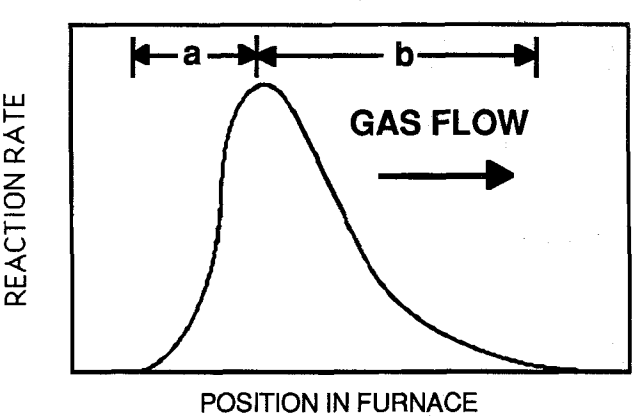

Fig. 5. Diagram indicating surface rate-limited entrance region (a), and mass-transfer and depletion-limited region (b).

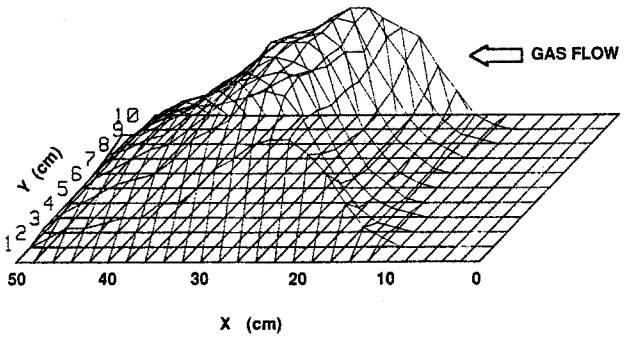

Fig. 6. Static deposition profile for carbon from IPA in N2. Peak height is 8 μm after 45 min deposition.

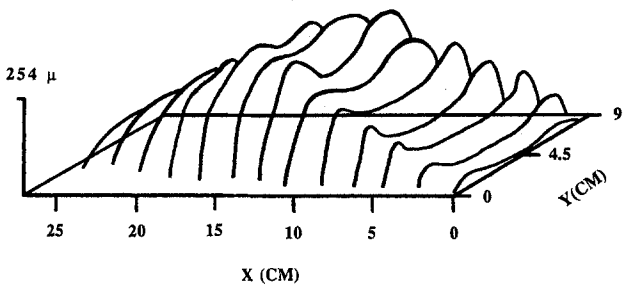

Fig. 7. Static deposition profile for silicon from TCS (trichlorosilane) in H_2.

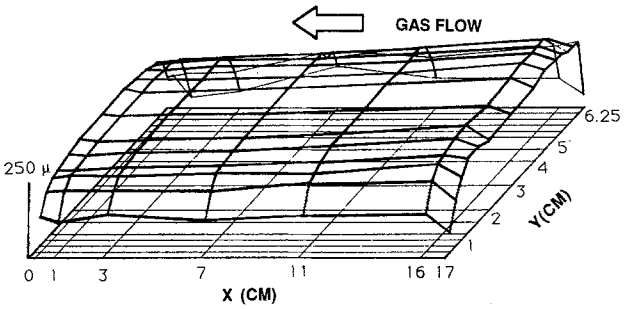

Fig. 8. Integrated silicon deposition profile with parallel partitions (gap = 2 mm).

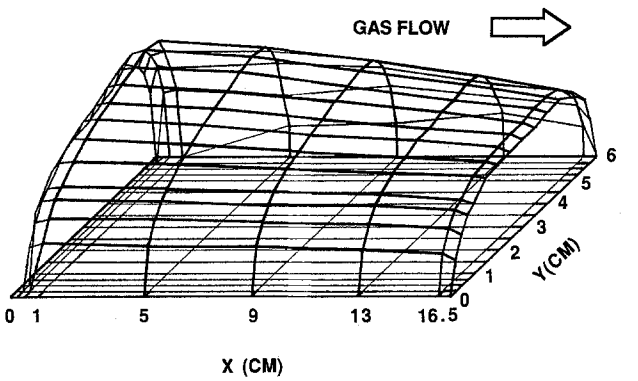

Fig. 9. Integrated silicon deposition with nonparallel partitions

order to deposit the same product thickness at the same furnace scan rate, the gas velocity must double. Assuming unchanged diffusion coefficients, we see that the length of the mass transport-limited and depletion-limited regions will be cut in half. The length of the surface rate limited region, determined by the steepness of the entrance thermal gradient, would not be affected.

Figures 6 and 7 show static deposition profiles for carbon and silicon, respectively. Much higher mass flow rates were used during silicon deposition than during carbon deposition, because of the necessary thicknesses of silicon (250 μm) and carbon (2 μm) to be deposited in comparable times. In addition, trichlorosilane (TCS) has a much higher heat capacity than IPA. Carbon and silicon static deposition profiles are therefore characteristic of low and high flow regimes, respectively. In the low flow regime, (Fig. 6), temperature varies little in the y direction, giving an almost one-dimensional deposition profile.

Deposition in the high flow regime can be best understood after a brief description of heat transfer. The partitioned box is heated mainly from the grooved sides, in order to make each partition see the same thermal environment. Heat conduction through the partitions is the largest component of heat transfer inside the box. Radiative heat transfer is inhibited as the partitions are packed closer together, because the mean free path for radiative transfer is proportional to the partition spacing. The result of heating the partitions at the edges and flowing cold gas up through them is U-shaped isotherms and deposition profiles, as can be seen in Fig. 7. In the entrance region, deposition occurs first at the hot partition edges, giving the inlet double peak. On the exit side, the edge gases are depleted first, resulting in a single peak in the center.

Integrated Deposition Profiles

The effect of scanning the furnace is to integrate the deposition profile and produce uniform deposition thickness. The same effect can be obtained by moving the boxes through a stationary furnace, which has the advantages of continuous rather than batch operation. The severe corrosion problems encountered with stainless steel exposed alternately to chloro-silanes and moist air made the scanning furnace system preferable by allowing all moving parts to be external to the corrosive gas stream.

The instantaneous deposition rate can be assumed to be some function $S(x, y)$ where x is in the reference frame of the furnace. Under the simplifying assumption that at steady state this function is constant and gets "dragged" along with the furnace, the integrated deposition thickness can be written

$$I(y) = \frac{1}{v}\int S(x, y)\, dx \qquad [6]$$

where the limits of integration extend over the entire nonzero portion of the instantaneous deposition rate. The instantaneous deposition rate $S(x, y)$ is different in the static and dynamic cases, because of the different thermal profiles resulting from the relative motion of furnace and boxes. The integal [6] is proportional to the quantity of reactant gas flowing over each part of the partition, and to the deposition efficiency of the reactor. The self-manifolding property of the partitioned box ensures equal gas flow over every part of the partition (neglecting the extreme edges, as mentioned previously). The effect of scan ning the furnace in the x direction is to integrate out the variations in the static profile and give a highly uniform integrated deposition profile.

Figure 8 shows an integrated silicon deposition profile. In this deposition, a uniform gap of 2 mm was used. To investigate the effect of nonuniform gap, partitions were shimmed to give a gap of 5 mm at one grooved box edge (y = 0) and a gap of 8 mm at the other edge (y = 6 cm) resulting in the deposition shown in Fig. 9. In this case, a gap ratio of 1.6:1 has resulted is a deposition ratio of only 1.4:1. Although Eq. [3] predicts a cubic dependence on gap, the observed typical variations are close to linear. This is because the gas flow in each channel is strongly influenced by the gas flow in the channels above and below it. During the experimental deposition shown in Fig. 9, only one box was shimmed, and in ribbon production the variations in gap spacing in one box were statistically uncorrelated with variations in the surrounding boxes. The cubic dependence on gap is therefore a worst-case which is rarely seen. Figure 9 clearly shows the need for tight tolerances on the partition and groove machining.

The most significant error made in the simplifying assumptions leading to [6] is that $S(x, y)$ remains constant. At startup and shutdown (top and bottom boxes) variations in $S(x, y)$ are unavoidable. The lack of thermal conduction at

the breaks between boxes distorts the thermal profile, tending to make each box isothermal. The net result is a slightly thicker deposit on the upstream side of each partition.

Conclusions

A novel CVD reactor for the growth of semiconductor polysilicon sheets and carbon films is reviewed. Gas flow through the reactor is analyzed to predict the effect of partition spacing on deposition uniformity. The scaling behavior of the deposition zones is examined as a function of process parameters. Techniques for avoiding homogeneous nucleation are presented. Thickness maps for both static and integrated depositions are shown. Silicon sheets produced in this reactor and released by the pyrocarbon oxidation undercut process (2) were used as feedstock for a solar cell process.

Acknowledgments

This work was performed at Solavolt International, which was a partnership of Motorola Solar Energy and SES (a subsidiary of Shell Oil), and to whom thanks are due for permission to publish. Thanks are also due to the Solavolt Equipment Engineering Group, especially Bill Smith and Larry Grenon, who designed four generations of CVD reactors, and to the Poly-Dep Group (Charles Chanley, T. Bruce Koger, and John Rice) for valuable discussions and experimental assistance.

Manuscript received Nov. 18, 1988.

REFERENCES

1. K. M. Lau and R. Dat, *IEEE Trans. Electron Device*, **ED-31** 1086 (1984).
2. J. J. Bernstein and T. B. Koger, *This Journal*, **135**, 2086 (1988).
3. R. W. Gurtler, A. Baghdadi, R. J. Ellis, and I. A. Lesk, *J. Electron. Mater.*, **7**, 441 (1978).
4. R. B. Bird, W. E. Stewart, and E. N. Lightfoot, "Transport Phenomena," pp. 80-81, John Wiley & Sons, New York (1960).
5. J. S. Newman, "Electrochemical Systems," pp. 311-322, Prentice Hall, Englewood Cliffs, NJ (1973).
6. M. H. Back and R. A. Back, in "Pyrolysis: Theory and Industrial Practice," L. F. Albright *et al.*, Editors, p. 21, Academic Press, Inc., New York (1983).
7. D. E. Brown, J. T. K. Clark, A. I. Foster, J. J. McCarroll, and M. L. Sims, in "Coke Formation on Metal Surfaces," L. F. Albright and R. T. K. Baker, Editors, pp. 23-43, A.C.S. Symposium Series no. 202, Washington, DC (1982).

Flow Characteristics of Novolak and PMIPK Type Photoresists in Baking Treatment as Related to Pattern Curvature

Makoto Morijiri,* Shinji Narishige, and Masanobu Hanazono

Hitachi Research Laboratory, Hitachi, Limited, Hitachi City, Ibaraki 319-12, Japan

Shin-ichi Hara, Harunobu Saito, and Masayuki Hayashi

Odawara Works, Hitachi, Limited, Odawara City, Kanagawa 256, Japan

ABSTRACT

We studied cross-sectional shape changes of two types of photoresists in postbaking treatment as related to the radius of pattern curvature, thickness, and postbaking temperature. Using a 140°-160°C postbaking treatment, novolak based photoresist patterns (thickness: 3-4 μm) lean and hang over toward the center of the pattern curvature. These phenomena were reflected in the small radius pattern curvature. On the other hand, for the same treatment the cross-sectional shape of the PMIPK type photoresist (thickness: 2.5-3.5 μm) was symmetric in the curvature. These phenomena were probably caused by the difference in surface tensions between the two types of photoresists. The PMIPK type photoresist was found to be well suited to use in redepositionless mask patterns for ion milling processing.

The ion milling method has come to be widely used in microelectronic circuit fabrications. Hanazono *et al.* (1) have fabricated thin film magnetic heads based on a dry process using the ion milling method. We have applied the ion milling method for the conductor coil windings of thin film magnetic heads.

Figure 1 shows a plane view of a thin film magnetic head, which is used in the Hitachi DK815-10 disk storage system. This head has double layered, 17-turn conductor coil windings with a pair of upper and lower magnetic yokes. The conductor coil windings are in the form of an elliptical oval shape. The radius of the pattern curvature of the conductor coil is the smallest in the innermost coil winding and the largest in the outermost one.

Using the ion milling method, there is a redeposition layer problem (2). When the angle of the cross-sectional shape of the photoresist pattern is large, the redeposition layer grows on the sidewall of the photoresist pattern. The redeposition layer is left behind on the etched pattern after the photoresist pattern is removed. To avoid this layer, the photoresist patterns are baked to round them and to decrease the angles of the cross-sectional shapes of the mask patterns (3).

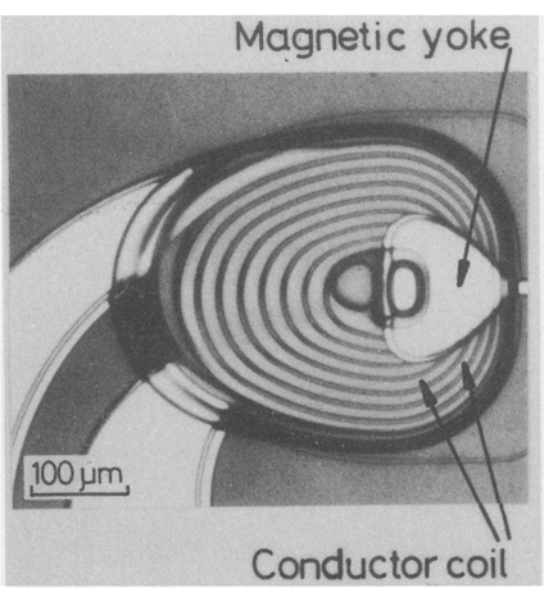

Fig. 1. A plane view of the thin film magnetic head

*Electrochemical Society Active Member.